A combined experimental and numerical approach for heat transfer enhancement in a minichannel using half rectified pulsating flows

Journal of Physics: Conference Series **2766** (2024) 012180 doi:10.1088/1742-6596/2766/1/012180

A combined experimental and numerical approach for heat transfer enhancement in a minichannel using half rectified pulsating flows

P S Kumavat[1], S Alimohammadi[1,2] and S M O'Shaughnessy[1]

[1] Department of Mechanical, Manufacturing and Biomedical Engineering, University of Dublin, Trinity College, Dublin, Ireland.
[2] School of Mechanical and Design Engineering, Technological University Dublin, Ireland.

Email: kumavatp@tcd.ie

Abstract. The miniaturization of electronic packages and their associated high-power density circuits requires more innovative cooling solutions. Single phase pulsating flows offer a promising solution due to their disruption of the thermal boundary layer. This study aims to bridge the knowledge gap by using experimental and computational methods to investigate the complex flow characteristics of laminar pulsating flows in a heated rectangular minichannel and couple that analysis with an investigation of thermal-hydraulic performance. Experimental analysis involves a uniformly heated thin foil approximating a constant heat flux bottom wall. Wall temperature measurements are recorded using an infrared thermography system. Analogous to the experimental conditions, a three-dimensional conjugate heat transfer computational model is developed with a volumetric heat generation source. Positive and negative half rectified sinusoidal pulsating flow waveforms are studied for dimensionless pulsation frequencies or Womersley numbers of $Wo = 2.5$ and 5.1 at a fixed flow rate amplitude $A_0 = 3$. For the positive half rectified waveform, a marginal enhancement in heat transfer of 2.2% for $Wo = 2.5$, $A_0 = 3$ was obtained. Whereas the negative half rectified case leads to a heat transfer enhancement of 9% and 6% for $Wo = 2.5$ and $Wo = 5.1$ respectively, with a high thermal performance of $\eta = 2.4$ over corresponding steady flow.

1. Introduction

The current and next generation energy dense micro-electronics packages require innovative liquid cooling solutions. Efficient cooling mechanisms are necessitated such that optimum performance levels are attained within safe temperature thresholds. Pulsating flows, consisting of an oscillating flow superimposed on a steady flow, are attracting more interest. Single-phase laminar pulsating flows are employed in several industrial applications owing to their distinct features such as unsteady fluid mixing and flow reversal effects leading to greater heat dissipation. Typical applications of pulsating flows include thermoelectric module cooling for battery thermal management systems [1], server-rack level component cooling, microchannel manifold heat sinks [2], micro-fluidic pulsed jet cooling [3] and pulse-tube cryocoolers.

Several dimensionless numbers are used to describe the pulsating flow characteristics. For a conduit of hydraulic diameter D_h, the steady flow Reynolds number, defined as $Re_s = VD_h/\nu$, represents the

ratio of inertial and viscous time scales. The Womersley number, $Wo = (D_h/2)\sqrt{(\omega/\nu)}$, quantifies the ratio of oscillating and diffusive time scales, where $\omega = 2\pi f$ is the oscillating angular velocity and f is the frequency [4]. The flow rate amplitude is defined as $A_0 = Q_{osc.max.}/Q_s$ and represents the ratio of the maximum oscillating flow rate ($Q_{osc.max.}$) to the steady flow rate (Q_s). A_0 can also influence the flow behaviour and heat transfer through flow reversal effects which typically occur at values $A_0 > 1$. To evaluate the thermal performance of pulsating flow, a time-space averaged Nusselt number $|\overline{\mathrm{Nu}}| = |\bar{h}|D_h/k$ defines the relationship between fluid thermal conductivity and surface convective heat transfer rate. The overall uncertainty in $|\bar{N}u|$ is about 6%, owing to higher uncertainties for wall and bulk temperatures. The heat transfer enhancement compared to the steady flow is given by $dNu = (|\overline{Nu}| - Nu_s)/Nu_s$, where Nu_s is the steady flow Nusselt number. To characterise the performance of half rectified flow pulsations in terms of heat transfer and pressure drop, a thermal performance parameter η is defined from equation (1), where the time averaged friction factor for pulsating flow ($\bar{\sigma}_p$) is obtained from Darcy–Weisbach equation, described in [5]. σ_s is the corresponding friction factor for steady flow at the same Re_s.

$$\eta = \left(\frac{\overline{Nu}_p}{Nu_s}\right)\left(\frac{\bar{\sigma}_p}{\sigma_s}\right)^{-1/3} \tag{1}$$

Recent studies have explored the potential for appreciable heat transfer enhancement using pulsating flows with modulated waveforms. Mehta and Khandekar [6] used square flowrate profiles in a uniformly heated minichannel with $0.8 \leq Wo \leq 5.9$ and $A_0 = 0.9$, indicating marginal heat transfer enhancement for high frequencies. Xu et al. [7] studied square, sawtooth, triangular, and sinusoidal excitation waveforms for nanofluid flow through microchannel heat sinks for frequencies $1 \leq f \leq 4.5$, with a maximum enhancement of 3.1% for a square waveform. Kumavat et al. [5,8] used asymmetric sinusoidal pulsating flows in a minichannel flow, determining 11% heat transfer enhancement over steady flow for $Wo = 5.1$ and $A_0 = 3$. The present study is based on a combined experimental and numerical investigation of unsteady half rectified sinusoidal pulsating flows. Experiments are performed using an Infrared thermography (IRT) technique to obtain time and space-resolved thermal measurements. Numerical simulations using a conjugate heat transfer model validate the experimental findings. The overarching aim is to exploit the characteristics of pulsating flow for efficient heat removal.

2. Experimental Methodology

More detailed discussions about the experimental technique are described in the earlier works by authors Kumavat et al. [5]. Here, a brief overview is provided. A 20 *mm* wide and 360 *mm* long rectangular minichannel is machined from Acrylic, resulting in an aspect ratio (AR) of 14.2 and hydraulic diameter of $D_h = 2.62\ mm$. A mechanically tensioned Inconel foil of 12.5 μm thickness forms the bottom surface of the minichannel and approximates a constant heat flux boundary when heated by a DC power supply. Foil thermal measurements are recorded non-intrusively using a calibrated high speed, high resolution FLIR SC6000 infra-red camera in conjunction with an IR transparent viewing window placed underneath the foil test section, which is located in the hydrodynamically and thermally developed region of the minichannel. IR recordings recording is initiated by an external TTL pulse trigger signal from LabVIEW to facilitate phase-locked measurements and the data is postprocessed in MATLAB. The minichannel with one heated long wall and all other walls insulated forms a H2(1L) duct thermal boundary condition [5]. A closed flow loop, as shown in figure 1, is supplied with de-ionized water. The hydrodynamic and thermal conditions at the inlet of the minichannel are carefully controlled. The maximum Reynolds number $Re_{max} = Re_s + Re_{osc,max} = 250$ provides a laminar flow with hydrodynamic and thermal entry lengths $L_e = 29\ mm$ and $Pr \times L_e = 204\ mm$, respectively.

The positive and negative rectified waveforms are generated through a complex flow control system that combines a three-way flow control valve and a scotch-yoke driven stepper motor system. The SMC VX3130-02N-5DZ1-B solenoid valve, as represented in figure 1, operates without a pressure differential requirement between its inlet and outlet ports and can respond to negative pressure circuits. The valve

is placed close to the exit of the stepper control system and is externally powered by a 24VDC supply. To execute a responsive switching of the magnetised coil, a MOSFET transistor is connected to the valve and the switching timing is programmed in LabVIEW to synchronise with the user desired pulsation frequency. E.g., to generate a positive half rectified oscillating flow component, a bypass loop re-routes the flow to the reservoir during the phases $0 \leq \theta \leq \pi$. While, for phases $\pi \leq \theta \leq 2\pi$, the flow entry into the minichannel is enabled from the scotch-yoke mechanism. A steady flow component is fed into the minichannel throughout the cycle, as illustrated in figure 1.

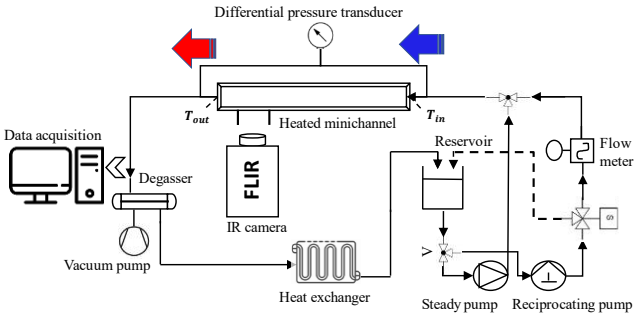

Figure 1. Schematic of the Experimental setup.

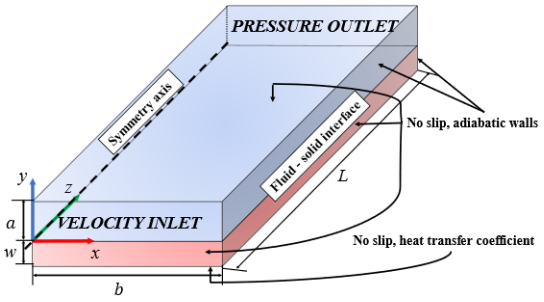

Figure 2. 3D computational domain and boundary conditions. Blue and red regions are fluid and solid domains respectively.

3. Numerical Methodology

Further details about the numerical methodology are elucidated in the earlier works by authors Kumavat et al. [9]. Using ANSYS CFX 2020 R2, a three-dimensional computational model with conjugate heat transfer is developed to approximate the experimental conditions, as presented in Figure 2. The geometry is composed of a cuboidal fluid domain with $360 \times 10 \times 1.4$ (in mm) with a 12.5 μm thick solid domain underneath of equal width and length. Water is specified as the working fluid with density of 1000 kg/m^3, dynamic viscosity of 8×10^{-4} $Pa \cdot s$, specific heat capacity of 4137 $J/kg \cdot K$ and thermal conductivity of 0.6 $W/m \cdot K$. The solid domain is defined as Inconel 600 with a density of 8420 kg/m^3, specific heat capacity of 444 $J/kg \cdot K$ and thermal conductivity of 14.9 $W/m \cdot K$. The solid is defined with a volumetric heat source of 3.6×10^8 W/m^3. A structured mesh consisting of 1,718,669 hexahedral elements with local refinements at the boundaries to capture the steep velocity and thermal gradients, is adopted. The inlet is specified with uniform temperature and a user defined function (UDF) defines the velocity profiles. A pressure outlet boundary condition is defined at the exit of the minichannel with 0 Pa as the gauge pressure. Top and side walls are approximated as no-slip and adiabatic for both the solid and fluid domains. The bottom surface of the solid domain is specified with a heat transfer coefficient to account for the heat losses from the underside of the heated foil surface, as shown in figure 2. A symmetry condition is imposed along the long face of the minichannel to reduce the computational requirements. Conjugate heat transfer problems in ANSYS CFX typically adopt a General Grid Interface technique that permits the creation of adaptable mesh connections across the solid-fluid interface. A mesh verification and validation study were previously carried out for symmetric sinusoidal waveforms (see Ref. [9]). A calculated Grid Convergence Index (GCI) index [10] of 1.2% is determined for the current work. Transient simulations are performed with an adaptive time-step such that solver stability and solution accuracy are dynamically controlled. The resulting time-step size varies between 10^{-3} and 10^{-4} and is dependent on the simulation case. Convergence of key parameters such as bottom wall temperature, mass flow, velocity components, is monitored and typically occurs after 20 pulsation cycles.

4. Results and Discussions

Figures 3 and 4 present a comparison of the data generated from experiments and CFD simulations. Generally, there exists a reasonable agreement between the datasets. Greater discrepancies exist at high

frequencies for the experimental measurements due to the amplified impulse produced from the solenoid control mechanism. Figure 3 (a-d) presents the temporal variation of normalized oscillating volumetric flow rate (Q_{osc}/Q_s), normalized pressure gradient ($\nabla p_{osc}/\nabla p_s$) and normalized wall shear stress (τ_{osc}/τ_s) in response to positive or negative half rectified waveforms for frequencies of $f = 0.5\ Hz$ ($Wo = 2.5$) and $f = 2\ Hz$ ($Wo = 5.1$) at the flow rate amplitude $A_0 = 3$. The positive half rectified waveform as shown in figure 3 (a, b) features a single pulsation with a steady component in the first half followed by a sinusoidal (net forward directed) component in the second half of the cycle. The effect of sinusoidal impulse is highlighted by the pressure gradient amplification observed with an increase in Wo. A phase lag is evident between the pressure gradient and flow rate profiles and an appearance of a distinct impulse in the pressure gradient profiles at phase π is observed. Contrastingly, with increasing Wo, a minimal effect on the magnitude of the normalized wall shear stress is noted, which lags the flow rate profile as the corresponding fluid velocities and velocity gradients increase.

The negative half rectified waveform as represented in figure 3 (c, d) presents a single pulsation with a steady component in the first half followed by a sinusoidal (net backward directed) component in the second half of the cycle. Increasing Wo, the effect of the shorter pulsation time period leads to a substantial amplification of the normalised pressure gradient. Additionally, a phase lag is developed with the flow rate profile and an increase in pressure gradient is evident at phase π, from figure 3 (d). An increase in phase lag is observed between the wall shear stress and flow rate profile rate and follows a similar understanding to the positive half rectified profile.

Figure 4 (a-d) shows the spanwise variation of the corresponding phase-averaged heated wall oscillating temperature profiles, where $T_{w,osc}$ is the difference between the time dependent and time averaged wall temperature. Data is obtained from the fully developed region of the channel at $z = 0.3\ m$. Lines and markers represent CFD and experimental data respectively, shown as a function of the non-dimensional minichannel width (x/b) along the heated wall (*i.e.*, at $y/a = 0$). Figure 4 (a, b) and (c, d) plots data for positive and negative half rectified waveforms respectively. The low frequency flow at $Wo = 2.5$ as noted from figure 4 (a) and (c) show higher magnitudes of temperature in the near side-wall regions $0.8 \leq x/b \leq 1$ compared to the core bulk regions. This is attributed to the presence of near wall viscous forces that continue to prevail in the convection dominant regime for the high pulsation flow rate amplitude of $A_0 = 3$. In the case of negative half rectified flow, figure 4 (c) shows higher temperature magnitudes as a result of a stronger flow withdrawal compared to the corresponding positive half rectified profile. With increasing Wo, as noted from figure 4 (b) and (d), the convection heat transfer is dominant and transverse diffusion is ineffective. The peak temperature magnitudes in the near side-wall vicinity decrease since the shear stress magnitudes are strengthened. The phenomenon of annular effects [8,11] widely noted for oscillating wall temperature profiles at high frequency are evident.

The calculated time-space averaged Nusselt number shows that heat transfer enhancement compared to steady flow is lower at the higher frequency $Wo = 5.1$ due to a reduced effect of transverse diffusion. $dNu\%$ values of 2% and 6% were respectively obtained for the positive and negative half rectified waveforms. At the lower frequency $Wo = 2.5$, peak heat transfer enhancement of 2.2% was determined for the positive half rectified waveform, whereas for the negative half rectified waveform, the backward driven flow showed a significant enhancement of 9%.

Compared to a steady flow, a high thermal performance is generally observed for both waveforms. At $Wo = 2.5$, a thermal performance of 1.4 is observed for the positive half rectified waveform and the performance decreases to 1.2 at $Wo = 5.1$. Whereas the negative half rectified attains a peak performance of 2.4 at $Wo = 2.5$ with a decrease to 1.8 at $Wo = 5.1$ due the underlying influence of greater shear stress magnitudes.

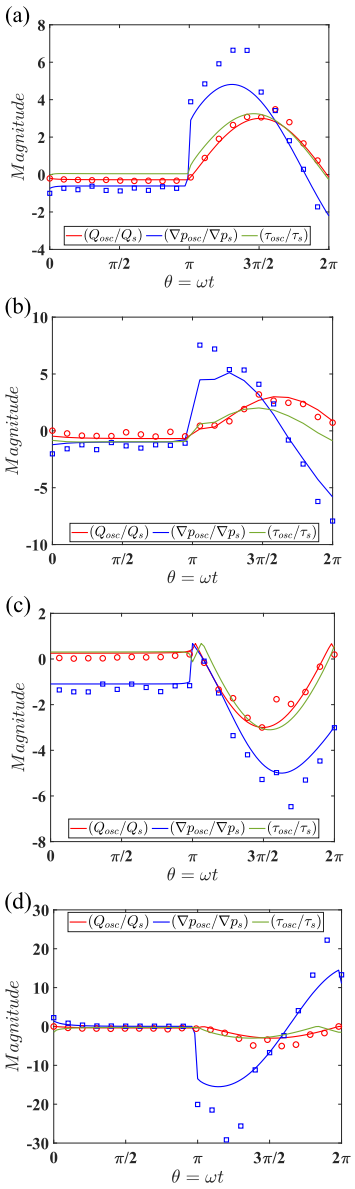

Figure 3. Temporal variation of the normalized oscillating flowrate, normalized oscillating axial pressure gradient, and normalized oscillating bottom wall shear stress (CFD only). Solid lines represent CFD data, markers show the experimental data. Half rectified sinusoidal waveforms with $A_0 = 3$. (a) $+ive,\ f = 0.5\ Hz,\ Wo = 2.5$, (b) $+ive,\ f = 2\ Hz,\ Wo = 5.1$, (c) $-ive,\ f = 0.5\ Hz,\ Wo = 2.5$, (d) $-ive,\ f = 2\ Hz,\ Wo = 5.1$.

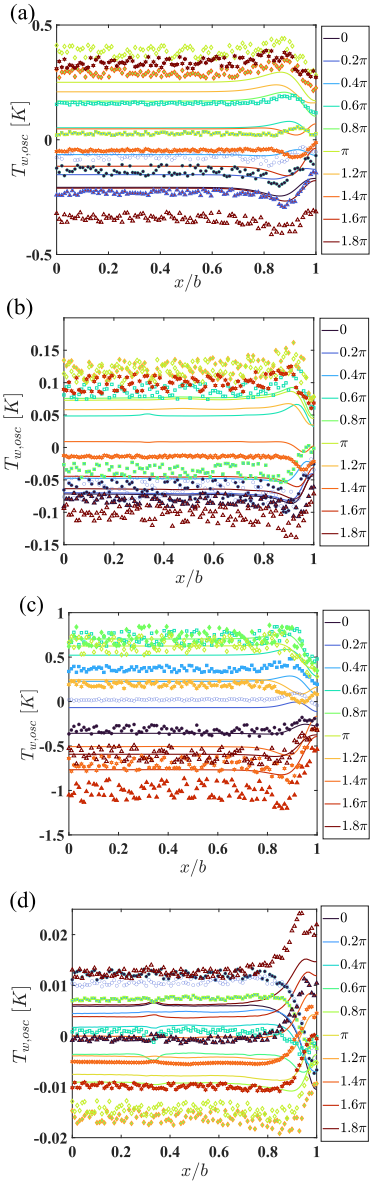

Figure 4. Oscillating temperature profiles at the heated wall ($y/b = 0$) along the normalized spanwise direction (x/a). Solid lines represent CFD data, markers show the experimental data. Half rectified sinusoidal waveforms with $A_0 = 3$. (a) $+ive,\ f = 0.5\ Hz,\ Wo = 2.5$, (b) $+ive,\ f = 2\ Hz,\ Wo = 5.1$, (c) $-ive,\ f = 0.5\ Hz,\ Wo = 2.5$, (d) $-ive,\ f = 2\ Hz,\ Wo = 5.1$.

5. Conclusions

Laminar pulsating flows of water with varying $Wo = 2.5$ and 5.1 at a flow rate amplitude of $A_0 = 3$ are experimentally and numerically investigated to evaluate the heat transfer potential. Positive and negative half rectified sinusoidal waveforms, each consisting of a half cycle of steady flow followed by a steady flow plus oscillating flow component, are investigated. As per the authors knowledge this forms the first spatial and temporal analysis of pulsating flows in a minichannel imposed with half rectified waveforms. Experiments are performed using infrared thermography to examine the transverse wall temperatures of a rectangular minichannel with bottom heated wall. A three-dimensional conjugate heat transfer model is developed with a volumetric heat generation approximating the experimental conditions. With an increase in Wo, the effect of sinusoidal impulse is widely evident thereby resulting in an amplification of pressure gradient. An increase in phase lag is observed between the flow rate and pressure gradient profiles while the effect on wall shear stress profiles is minimum. The corresponding spanwise phase-averaged oscillating wall temperatures for low frequency flow reflect greater magnitudes in the near side-wall vicinity. Whereas for a convection dominant high frequency flow, transverse diffusion is ineffective leading to decreased near side-wall temperature magnitudes. A peak heat transfer enhancement of 9% and a peak thermal transfer performance of 2.4 over steady flow is obtained for negative half rectified pulsating waveform at $Wo = 2.5, A_0 = 3$.

Acknowledgements

The authors would like to thank the University of Dublin, Trinity College, for their financial support as well as the Irish Centre for High End Computing (ICHEC) for their computational support and facilities under project tceng025c.

References

[1] Sirikasemsuk S, Wiriyasart S, Prurapark R, Naphon N and Naphon P 2021 *Int. J. Heat Technol.* **39** 5 pp 1618–26
[2] Zhang H, Li S, Cheng J, Zheng Z, Li X and Li F 2018 *Appl. Therm. Eng.* **129** pp 1092–105
[3] de Bock H P, Chamarthy P, Jackson J L and Whalen B 2012 *13th InterSociety Conference on Thermal and Thermomechanical Phenomena in Electronic Systems* p 1387–94
[4] Womersley J R 1955 *J. Physiol.* 1955 **127** 3 pp 553–63
[5] Kumavat P S, Alimohammadi S and O'Shaughnessy S M 2023 *IEEE Trans. Components, Packag Manuf. Technol.* 2023 1
[6] Mehta B and Khandekar S 2015 *Int. J. Therm. Sci.*
[7] Xu C, Xu S, Wang Z and Fenga D 2021 *Int. Commun. Heat Mass Transf.* **125** p 105343
[8] Kumavat P amd O'Shaughnessy S M 2021 J. Phys. Conf. Ser. **2116** 1 p 012031
[9] Kumavat P S, Alimohammadi S and O'Shaughnessy S M 2022 *Int. J. Therm. Sci* **182** p 107790
[10] Celik I B, Ghia U, Roache P J, Freitas C J, Coleman H and Raad P E 2008 *J. Fluids Eng. Trans. ASME.* **130** 7 pp 0780011–4
[11] Blythman R, Alimohammadi S, Jeffers N, Murray D B and Persoons T 2022 *J. Heat Transfer* **144** 1 pp 1–9